

Fore-Aft Oxygen Storage Control

Giovanni Fiengo¹, Jeffrey A. Cook² and J. W. Grizzle³

Abstract

This paper describes model-based, active control of an aftertreatment system for a spark ignition engine equipped with a three-way catalyst (TWC) and pre- and post-TWC oxygen sensors. A controller is designed to manage the oxygen storage level in the TWC in order to maximize the simultaneous conversion efficiencies of oxides of nitrogen, NO_x , unburned hydrocarbons, HC , and carbon monoxide, CO . Linear exhaust gas oxygen sensors (UEGOs) are used to measure pre- and post-catalyst A/F . The pre-catalyst A/F measurement is assumed to be biased in addition to being corrupted by zero-mean noise, while the post-catalyst measurement is assumed to be only corrupted by zero-mean noise. A series controller configuration is adopted. The upstream controller provides relatively rapid response to disturbances on the basis of the pre-catalyst measurement, while the downstream controller uses an extended Kalman filter (observer) to estimate the relative oxygen level of the TWC on the basis of the pre- and post-catalyst A/F measurements. The estimated value of oxygen storage is then used to regulate the relative oxygen level of the TWC to 50%. The performance and robustness of the proposed control system in the face of noise and model uncertainty are evaluated through extensive simulations.

1 Introduction

Conventional automotive gasoline engines employ a three-way catalytic converter to oxidize HC and CO emissions, and reduce NO_x . Traditionally, the control emphasis has been on A/F feedback using an exhaust gas oxygen (EGO) sensor located in the exhaust manifold upstream of the TWC to maintain the A/F near stoichiometry and achieve high simultaneous conversion efficiencies. Recent requirements for onboard diagnostics (OBD) have led to the placement of an additional EGO sensor downstream of the TWC. This

secondary sensor is often used to trim the control action of the primary sensor. The catalyst dynamics, however, are not typically considered in the design of the control system, whether using one or both sensors. The goal of this paper is to develop steady-state, active control of the aftertreatment system using the pre- and post-catalyst oxygen sensors to improve both performance and robustness. In this context, steady-state refers to conditions of constant engine speed and air flow rate.

Figure 1 illustrates the system to be controlled. The upstream and the downstream oxygen sensors are universal, or linear EGO (UEGO) sensors. Section 2 describes the models of the internal combustion engine (ICE) and the EGO sensors. The TWC model is described in [1]; for other models, see [4, 11]. Subsequent sections describe controller design and investigate robustness for the system.

The work most similar to this paper is [6]. On the basis of a limited integrator model of the TWC, an oxygen storage estimator was designed and subsequently used in a PI-based adaptive feedback control strategy. The control system effectively regulated the oxygen storage level of the catalyst to a limit cycle about the half-full point. The limit cycle, however, had rather large amplitude in the feedgas A/F , which leads to driveability problems. One of the goals of the present work is to use a more advanced controller design scheme to minimize the amplitude of any limit cycles. In addition, the present work directly addresses the non-equilibrium effects in the exhaust gas which can result in a bias error in the air-fuel ratio sensor upstream of the catalyst.

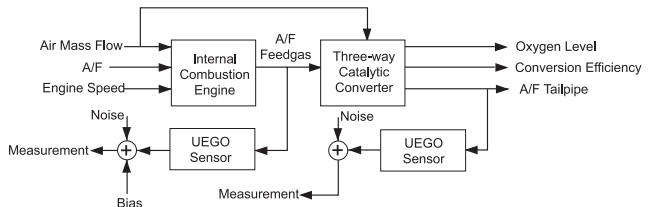


Figure 1: Engine and Catalyst.

2 Model

2.1 Internal Combustion Engine

In steady-state, the ICE A/F subsystem may be simply modeled as the speed dependent induction-to-exhaust

¹Giovanni Fiengo is with the Computer and System Engineering Department, Università di Napoli Federico II, Naples, Italy. E-mail: gifiengo@unina.it

²Jeffrey A. Cook is with Ford Research Laboratory, P.O. Box 2053, MD 2036 SRL, Dearborn, MI 48121, USA. E-mail: jcook2@ford.com

³Jessy W. Grizzle is with the Electrical Engineering and Computer Science Department, University of Michigan, Ann Arbor, MI 48109-2122, USA. E-mail: grizzle@umich.edu

stroke delay of the four-stroke cycle cascaded with transport delays in the exhaust system from the exhaust valve to the upstream EGO sensor, from the EGO sensor to the catalyst, the catalyst delay and a delay from the catalyst to the downstream sensor. For the particular system modeled here, the transport delay to the first sensor is lumped with the speed-dependent engine delay, the catalyst delay is lumped with the transport delay after the first EGO, and the delay from the catalyst to the downstream EGO is considered negligible. For a four-cylinder engine sampled at an event interval (induction-compression-expansion-exhaust) of 180 crankshaft degrees, the sample time, dt , at 1500 rpm is 0.02 sec and the engine delay is 0.08 sec. The lumped delay to the upstream sensor (engine plus transport) is 6 dt or 0.12 sec. The lumped catalyst and transport delay after the sensor is 0.08 sec.

2.2 Air-Fuel Ratio Sensor

As shown in Figure 1, the engine is equipped with two UEGO sensors to measure the quantity of oxygen in the exhaust gas at the feedgas and at the tailpipe. These sensors provide an actual measurement of the oxygen content in the exhaust. Importantly, feedgas and tailpipe A/F measurements are affected by different types of inaccuracy. Upstream of the catalyst, non-equilibrium effects in the exhaust gas result in a bias error in the sensor [12, 2, 10, 7, 8]. This bias is due in part to incomplete catalysis of CO on the sensor substrate and in lesser part to NO_x ; an additional confounding factor is the large discrepancy in the diffusion rate of H_2 with respect to other species present in the exhaust gas. Assuming thermodynamic equilibrium in the exhaust gas after the catalyst, the measurement disturbance at the tailpipe A/F sensor is considered to be zero mean white noise. Finally, the linear sensor is modeled as a first order system with unit gain and time constant τ_u equal to 250 ms , as represented in the transfer function

$$\lambda_u = \frac{1}{1 + s\tau_u}\lambda, \quad (1)$$

where λ_u is the measured variable and λ is the actual A/F in the feedgas or in the tailpipe.

3 Control

In this section, a feedback controller is designed having two objectives: first, to simultaneously maximize the conversion efficiencies of HC , CO and NO_x ; and second, to obtain steady-state air-fuel control which is robust with respect to disturbances, but which minimizes excursions around stoichiometry. The standard feedforward control action based on measured or estimated mass air flow rate is not discussed [3, 9].

The controller is formed by two blocks connected in se-

ries (see Figure 2). The first block, the *Fore Controller*, feeds back the output of the first sensor and the second block, the *Aft Controller*, feeds back the measurements from the first and second sensors. The fore controller is a PI with anti-windup; it responds relatively quickly to A/F disturbances. The aft controller consists of two principal parts: a *Bias Estimator* that processes both pre- and post-TWC UEGO measurements to estimate the persistent bias in the pre-TWC UEGO sensor, and an *extended Kalman filter* to estimate the stored oxygen level of the TWC. The objective of the aft-controller is to maintain the relative oxygen storage level of the TWC at 50%; it acts on a slower time scale commensurate with the longer measurement delay in the second sensor.

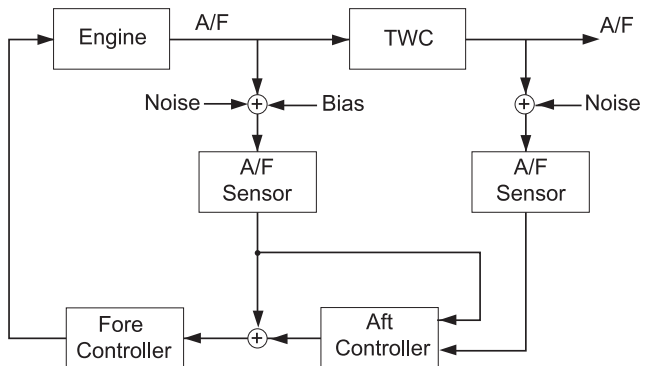


Figure 2: Fore-Aft Controller - Series Configuration.

3.1 PI Controller

The design of the PI controller is based on the model, $P(s) = e^{-0.12s}$. Classical design rules were used to select the gains so as to trade off speed of response with gain and phase margins. Since typically a limiter is placed on the output of the controller, anti-windup is used to turn off the integral action as soon as the actuator saturates, which reduces both overshoot and control effort in the feedback system. The base reference signal for the fore PI controller is stoichiometry. This will be modified by the aft controller in view of its objective to regulate the relative oxygen level of the catalyst.

3.2 Bias Estimator

The basic idea of the bias estimator is that the average A/F in the feedgas and tailpipe should be the same if the feedgas signal remains constant for a sufficiently long period of time. That is, if λ_{FG} is constant at a lean value, λ_{TP} will reach the same value when the catalyst is completely filled with oxygen. Conversely, if λ_{FG} is rich, λ_{TP} and λ_{FG} will be equal after the catalyst has been entirely depleted of oxygen. At stoichiometry, λ_{TP} equals λ_{FG} , independently of the oxygen state of the catalyst. To enable a comparison between the output of the two sensors, the feedgas signal should be constant for a time sufficient to fill an empty cata-

lyst with oxygen or, conversely, to deplete a filled one. Hence, in steady-state, differences in the averaged values of the two measurements are due to the bias in the upstream sensor. To assure steady-state operation, the estimation of the bias is updated only if the average measurement of the feedgas A/F remains almost constant for some time, Δ seconds. The output of the bias estimator is subtracted from the output of the upstream UEGO sensor before it is used by any of the controllers.

3.3 Kalman Filter

This section summarizes the design of a steady-state, extended Kalman filter to estimate the oxygen storage level of the catalyst. The system to be observed is composed of the internal combustion engine in series with the catalytic converter. For the engine, delays are modeled as a first order Padé approximations. The two series delays, one of 0.12 sec and the other of 0.08 sec, are represented by the following state-space systems:

$$\begin{cases} \dot{x}_1 = -16.6667x_1 + 8\lambda \\ \lambda_E = 4.1667x_1 - \lambda \end{cases}, \quad (2)$$

$$\begin{cases} \dot{x}_2 = -25x_2 + 8\lambda_E \\ \lambda_{FG} = 6.25x_2 - \lambda_E \end{cases}, \quad (3)$$

where λ , the air-fuel ratio in the cylinders, is the sum of the A/F requested by the fore-controller, λ_{con} , and the combined uncertainty of the air-charge estimate and the fuel injectors, λ_{ac} ,

$$\lambda = \lambda_{con} + \lambda_{ac}; \quad (4)$$

λ_E is the A/F ratio after the first delay (corresponding to the engine delay plus the exhaust manifold delay), and is the input to the sensor; λ_{FG} is the feedgas A/F , which is the input to the TWC; x_1 and x_2 are the states respectively of the state-variable representation of the first and the second delays (recall that the second delay is the transport delay between the sensor and the catalyst). The overall system to be observed is a sixth order nonlinear system described by the following equations:

$$\begin{cases} \dot{x}_1 = -16.6667x_1 + 8(\lambda_{con} + \lambda_{ac}) \\ \dot{x}_2 = -25x_2 + 8[4.1667x_1 - (\lambda_{con} + \lambda_{ac})] \\ \dot{\lambda}_{ac} = 0 \\ \dot{\lambda}_{u_1} = -\frac{1}{\tau_u}\lambda_{u_1} + \frac{1}{\tau_u}[4.1667x_1 - (\lambda_{con} + \lambda_{ac})] \\ \dot{\Theta} = \begin{cases} \frac{1}{C(MAF)} \times \rho(\lambda_{FG}, \Theta) \times 0.23 \times \\ MAF \times \left(1 - \frac{1}{\lambda_{FG}}\right) & 0 \leq \Theta \leq 1 \\ 0 & \text{otherwise} \end{cases} \\ \dot{\lambda}_{u_2} = -\frac{1}{\tau_u}\lambda_{u_2} + \frac{1}{\tau_u}\lambda_{TP} \end{cases} \quad (5)$$

$$\begin{aligned} \lambda_E &= 4.1667x_1 - (\lambda_{con} + \lambda_{ac}) \\ \lambda_{FG} &= 6.25x_2 - [4.1667x_1 - (\lambda_{con} + \lambda_{ac})] \\ \lambda_{TP} &= \lambda_{FG} - \rho(\lambda_{FG}, \Theta) \times (\lambda_{FG} - 1) \end{aligned} \quad (6)$$

where $\rho(\lambda_{FG}, \Theta)$ is described in [1]. The system has one input, λ_{con} , that is the control signal coming from the fore-controller, three non-measured outputs, λ_E , λ_{FG} and λ_{TP} , and two measured outputs, λ_{u_1} and λ_{u_2} ; the measured outputs are corrupted by white noise. The states are x_1 and x_2 coming from the Padé approximations, the actuator uncertainty λ_{ac} , the output of the two sensors λ_{u_1} and λ_{u_2} , and the relative oxygen level Θ .

With the state variable λ_{ac} , the Kalman filter attempts to estimate the uncertainty of the injectors to provide the desired quantity of fuel. Since the engine is operating in steady-state, the uncertainty is assumed to be constant or slowly varying and, consequently, has zero derivative. It is not possible to distinguish the bias of the upstream UEGO sensor from the uncertainty of the engine using only the measurement from the upstream sensor. To obviate this problem, the Kalman filter uses the output of the upstream sensor corrected by the bias estimator. Hence, the remaining estimation error of the bias is included in the estimation of the engine uncertainty.

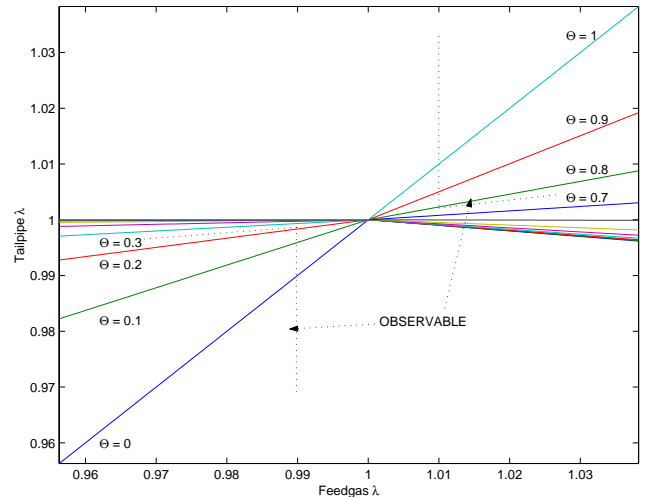


Figure 3: λ_{TP} as a function of λ_{FG} for different values of the relative oxygen level Θ .

The major challenge in designing the estimator is that the TWC is not uniformly observable. This is illustrated in Figure 3 which shows the instantaneous relationship between tailpipe versus feedgas air-fuel ratio for different levels of oxygen storage in the catalyst. In particular, under rich conditions, the TWC is almost unobservable when the relative oxygen level is greater than 0.2; under lean conditions, the relative oxygen level must be larger than 0.8 to be strongly observable from the available signals. Thus, when the oxygen storage level, Θ , is regulated in the desired range, it is practically impossible to observe it based on the downstream UEGO signal. Consequently, the Kalman filter gain between the TWC and the second UEGO was

computed for the observable and weakly observable operating regimes using different weights in the algebraic Riccati equation.

The filter design is completed by linearizing the model to obtain (A, C) as a function of the states and computing a steady-state Kalman gain via the algebraic Riccati equation

$$0 = P_e A^T + A P_e - P_e C R^{-1} C^T P_e + Q \quad (7)$$

$$K_e = P_e C R^{-1}. \quad (8)$$

The weights Q and R on the states and outputs, respectively, were selected to emphasize the model in the region where it is poorly observable and the outputs in the region where it is strongly observable. In total, the Kalman gain K_e was evaluated for the linearized system at 20 (Θ, λ_{FG}) operating points and stored in a look-up table. The look-up table was then interpolated over the estimated trajectory in order to reduce the computational burden.

Defining the difference between the measured (λ_{u_i}) and the estimated $(\hat{\lambda}_{u_i})$ variables as

$$err_e = \begin{pmatrix} \lambda_{u_1} - \hat{\lambda}_{u_1} \\ \lambda_{u_2} - \hat{\lambda}_{u_2} \end{pmatrix}, \quad (9)$$

the equations of the extended Kalman observer are the following:

$$\begin{cases} \dot{\hat{x}}_1 = -16.6667\hat{x}_1 + 8(\lambda_{con} + \hat{\lambda}_{ac}) + K_e \cdot err_e \\ \dot{\hat{x}}_2 = -25\hat{x}_2 + 8[4.1667\hat{x}_1 - (\lambda_{con} + \hat{\lambda}_{ac})] \\ \quad + K_e \cdot err_e \\ \dot{\hat{\lambda}}_{ac} = K_e \cdot err_e \\ \dot{\hat{\lambda}}_{u_1} = -\frac{1}{\tau_u}\hat{\lambda}_{u_1} + \frac{1}{\tau_u}[4.1667\hat{x}_1 - (\lambda_{con} + \hat{\lambda}_{ac})] \\ \quad + K_e \cdot err_e \\ \dot{\hat{\Theta}} = \begin{cases} \frac{1}{C(MAF)} \times \rho(\hat{\lambda}_{FG}, \hat{\Theta}) \times 0.23 \times MAF \\ \times \left(1 - \frac{1}{\lambda_{FG}}\right) + K_e \cdot err_e & 0 \leq \hat{\Theta} \leq 1 \\ 0 & \text{otherwise} \end{cases} \\ \dot{\hat{\lambda}}_{u_2} = -\frac{1}{\tau_u}\hat{\lambda}_{u_2} + \frac{1}{\tau_u}\hat{\lambda}_{TP} + K_e \cdot err_e \end{cases} \quad (10)$$

$$\hat{\lambda}_{FG} = 6.25\hat{x}_2 - [4.1667\hat{x}_1 - (\lambda_{con} + \hat{\lambda}_{ac})] \quad (11)$$

$$\hat{\lambda}_{TP} = \hat{\lambda}_{FG} - \rho(\hat{\lambda}_{FG}, \hat{\Theta}) \times (\hat{\lambda}_{FG} - 1) \quad (12)$$

3.4 Aft-Controller

The aft-controller consists of proportional control on the difference between the estimated oxygen storage level and its desired value, here, taken to be 0.5:

$$\lambda_{aft} = K(\hat{\Theta} - 0.5). \quad (13)$$

The output of this controller is used to adjust the reference going into the upstream PI controller. Other controller design methods (such as LQG) and controller configurations (such as inner-outer) were also investigated but are not reported here for lack of space.

4 Simulation Results

For the catalyst model, the steady-state conversion efficiencies at stoichiometry were assumed to be $HC=96.75$ $NOx=97.15$ and $CO=99.4$. The goal is to achieve these values in the face of significant measurement uncertainty in the upstream UEGO sensor and significant error in the estimated air-charge and/or fuel injection quantity. Injector and air-charge estimation uncertainty has been simulated by summing the signal shown in Figure 4 with the output of the PI controller. A bias equal to -0.2 A/F is assumed for the upstream UEGO. White noise disturbances taking values between $\pm 0.5\%$ of stoichiometry are applied to the UEGO sensors.

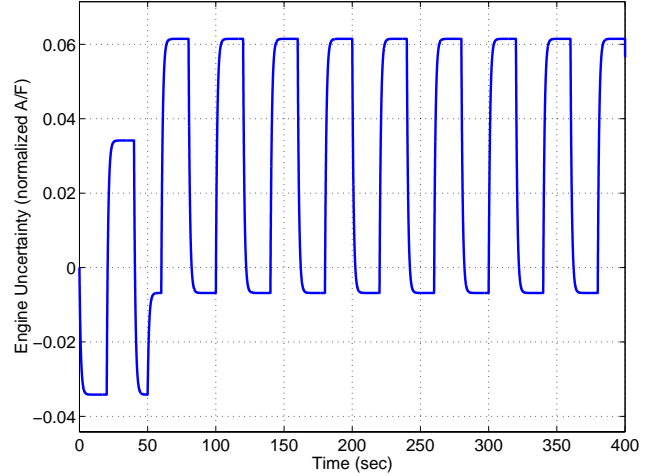


Figure 4: Combined injector and air charge uncertainty in units of normalized A/F .

Simulation results are shown in Figures 5 - 7. The controller shows excellent performance. Even in the presence of very significant uncertainty, the tailpipe A/F is regulated very closely to stoichiometry, and very nearly achieves the maximal possible average simultaneous conversion efficiencies of the three main pollutants. Moreover, the variance of the feedgas A/F is small (see Figure 5), indicating that there should be no driveability problems due to the actions of the controller. The remaining figures show simulated and estimated oxygen storage level, and the actual and estimated bias level.

5 Robustness Analysis

This section addresses the robustness of the controller. For this purpose, while holding all values in the controller fixed, the bias, measurement noise and injector uncertainty disturbances were increased, and the oxygen storage capacity of the catalyst and the engine time delays were modified. To further evaluate robust-

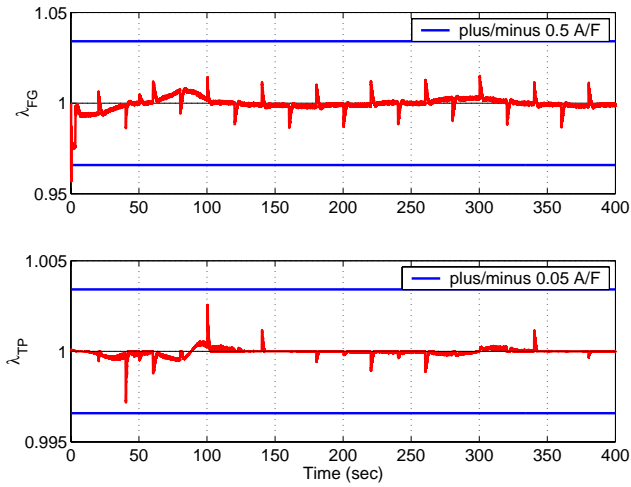


Figure 5: Feedgas, λ_{FG} , and tailpipe, λ_{TP} , air-fuel ratios.

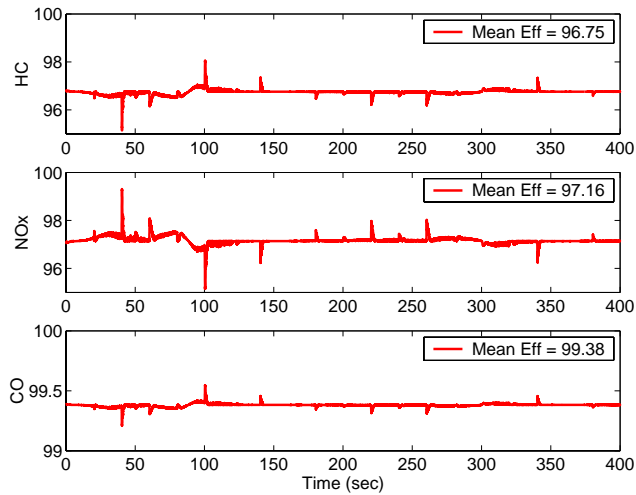


Figure 6: Conversion efficiencies of HC , NO_x and CO .

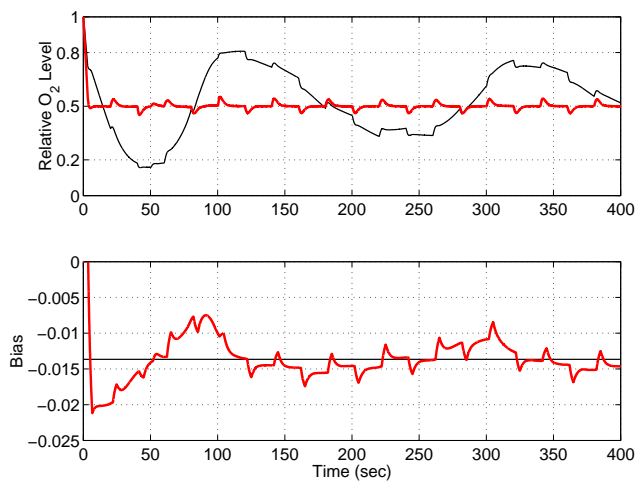


Figure 7: Relative oxygen level, Θ , and upstream UEGO sensor bias. The thin lines are the actual values and the bold lines are the estimated values.

ness to model uncertainty, a completely different TWC representation (described in [5]) from that used in the controller was inserted in the simulation model and the position of the second A/F sensor was changed by inserting a delay equal to 0.08 sec between the TWC and this sensor. For conciseness of presentation, the results of the simulations are tabulated with respect to the conversion efficiencies for NO_x , HC , and CO , and the mean and standard deviations of the tailpipe and feedgas air-fuel ratios. For a baseline, the first column of Table 1 contains the performance metrics for the controller subjected to the standard disturbances and uncertainties of Section 4: bias equal to -0.2 A/F at stoichiometry; white noise sensor disturbance between $\pm 0.5\%$ of stoichiometry, and injector uncertainty as illustrated in Figure 4. The time delays and the oxygen storage capacity of the catalyst are fixed to values of Section 2 and [1], respectively.

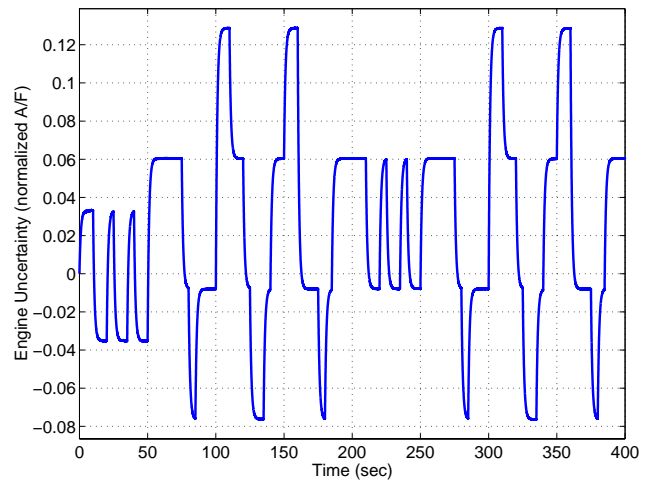


Figure 8: Combined injector and air charge uncertainty, in units of normalized A/F , that is used in one part of the robustness analysis.

In the robustness investigation, the various perturbations are first applied separately. The second column of Table 1 shows the simulation results for bias equal to -0.4 A/F, white noise sensor disturbance between $\pm 1\%$ of stoichiometry, and injector uncertainty as shown in Figure 8. The results in the third column are obtained using the *standard* disturbances enumerated in the previous paragraph, but decreasing by 50% the oxygen storage capacity, thereby simulating the aging of the catalyst.

The performance of the system when the engine delays and the sensor placement are changed is illustrated in the fourth column of Table 1. The fifth column reports results when the modified catalyst dynamics are substituted. Finally, the last column provides the results when all of the changes are applied simultaneously.

	Base-Line	Disturb	TWC Cap.	Delays	TWC Model	All Together
HC Eff.	96.75	96.72	96.76	96.75	96.76	96.72
NO_x Eff.	97.16	97.13	97.13	97.12	97.14	97.08
CO Eff.	99.38	99.38	99.38	99.38	99.38	99.38
λ_{FG} mean	1.000	1.000	1.000	1.000	1.000	1.000
λ_{FG} std. dev.	3.1e-3	6.7e-3	2.9e-3	3.8e-3	3.1e-3	7.9e-3
λ_{TP} mean	1.000	1.000	1.000	1.000	1.000	1.000
λ_{TP} std. dev.	2.0e-4	5.5e-4	3.6e-4	4.2e-4	2.3e-6	6.2e-4

Table 1: Robustness analysis comparing the base-line results of Section 4 to successive changes in the disturbance and noise levels, oxygen storage capacity of the catalyst, time delays in the model, choice of catalyst oxygen storage model, and, finally, imposing all of the uncertainties at once.

6 Conclusions

The controller shows good performance and considerable robustness to changes in system parameters. This design has also been tested on different catalyst configurations, including a series of two TWCs (close-coupled plus under-body TWC) and a Y-configuration (two close-coupled and one under-body TWC). The results obtained in these configurations show similar improvements in performance and robustness.

Acknowledgments

J.W. Grizzle gratefully acknowledges funding under a Ford Motor Company URP titled *Active Control of Aftertreatment for Improved Emissions and Fuel Economy*.

References

- [1] E.P. Brandt and Y. Wang and J.W. Grizzle, "Dynamic Modeling of a Three-Way Catalyst for SI Engine Exhaust Emission Control," *IEEE Transactions on Control System Technology*, vol. 8, No. 5, September 2000.
- [2] A. D. Colvin and J. W. Butler and J. E. Anderson, "Catalytic Effects on ZrO₂ Oxygen Sensors Exposed to Non-Equilibrium Gas Mixtures," *J. Electroanal. Chem.*, number 136, 1982.
- [3] J.A. Cook, J.W. Grizzle and J. Sun, "Automotive Engine Control," *The Control Handbook*, CRC Press, W. Levine, Ed., 1996, pp. 1261-1274.
- [4] C. Cussenot and M. Basseville and F. Aimard, "Monitoring the Vehicle Emission System Components," *IFAC 13th Triennial World Congress*, June 1996.
- [5] G. Fiengo, L. Glielmo and S. Santini, "On Board Diagnosis for Three-Way Catalytic Converters," *International Journal of Robust and Nonlinear Control*, Vol. 11, No. 11, September, 2001, pp. 1073-1094.
- [6] E. Shafai and C. Roduner and H.P. Geering, "Indirect Adaptive Control of a Three-way Catalyst," SAE paper 961038, February 1996.
- [7] H. J. Germann, C. H. Onder and H. P. Geering, "Fast Gas Concentration Measurements for Model Validation of Catalytic Converters," SAE paper 950477, February 1997.
- [8] H. Germann, S. Tagliaferri and H. P. Geering, "Differences in Pre- and Post-Converter Lambda Sensor Characteristics," SAE paper 960335, February 1996.
- [9] J.W. Grizzle, J.A. Cook and W.P. Milam, "Improved Cylinder Air Charge Estimation for Transient Air Fuel Ratio Control," *1994 American Control Conference*, Baltimore, June 1994.
- [10] D. R. Hamburg, J. A. Cook, W. J. Kaiser and E. M. Logothetis, "An Engine-Dynamometer Study of the A/F Compatibility Between a Three-way Catalyst and an Exhaust Gas Oxygen Sensor," SAE paper 830986, June 1983.
- [11] K. N. Pattas, A. M. Stamatelos, P. K. Pistikopoulos, G. C. Koltsakis, P. A. Konstandinidis, E. Volpi and E. Leveroni, "Transient Modeling of 3-Way Catalytic Converters," SAE paper 940934, February 1994.
- [12] M. A. Shulman and D. R. Hamburg, "Non-ideal Properties of ZrO₂ and TiO₂ Exhaust Gas Oxygen Sensors," SAE paper 800018, February 1980.